J. Materials, Conc. Struct. Pavements, JSCE, No. 760/V-63, 279-288, 2004 May

STRUCTURAL DAMAGE IDENTIFICATION OF CONCRETE SPECIMEN IN PROGRESSIVE FAILURE

Katsuichiro GODA[1], Akira KOBAYASHI[2] and Shigeyasu AOYAMA[3]

[1]Student Member of JSCE, Graduate Student, Graduate School of Agriculture, Kyoto University
(Oiwake-cho, Kitashirakawa, Sakyo-ku, Kyoto 606-8202, Japan)
[2]Member of JSCE, Dr. Eng., Associate Professor, Graduate School of Agriculture, Kyoto University
(Oiwake-cho, Kitashirakawa, Sakyo-ku, Kyoto 606-8202, Japan)
[3]Member of JSCE, Dr. Agr., Professor, Graduate School of Agriculture, Kyoto University
(Oiwake-cho, Kitashirakawa, Sakyo-ku, Kyoto 606-8202, Japan)

The structural damage identification method using genetic algorithm, which estimates the location and severity of inflicted damage by considering natural frequencies and inferred damage patterns has been proposed by the authors. In this paper, the validity of this method is tried by applying it to the estimation of the progress of damage due to cyclic uniaxial loading of a rectangular concrete specimen. At each loading stage, impact sounds and acoustic emissions are measured. By using these as a priori information, the decreased degree of elastic modulus is estimated. By implementing it successively, it is possible to estimate the progress of damage.

Key Words : *successive damage identification, genetic algorithm, test verification, acoustic emissions*

1. INTRODUCTION

A structural damage identification method[1),2)] using genetic algorithm[3)] (GA), which can estimate the location and severity of inflicted damage using a priori information on natural frequencies and inferred damage patterns has been proposed by Goda et al.[4)]. This method identifies the decreased degree of elastic modulus (hereafter, E.M.) of damaged areas. Through the sensitivity analysis on a priori information, the following conclusions are found: it is difficult to obtain a good estimation when only a priori information on natural frequencies is available and, estimation accuracy will increase when better a priori information on the location of damage is available rather than its severity.

In this paper, this method is applied to an experimental problem and the estimation of the progress of damage due to cyclic uniaxial loading is examined by the proposed method. In an experiment, a rectangular concrete specimen (10×10×40cm) undertakes cyclic loading which increases gradually until its failure. As a cycle, the specimen is loaded to a given stress value at a constant strain ratio and then unloaded to zero stress. Acoustic emissions, applied load and both vertical and horizontal strains by strain gauges are measured while loading, and the impact sounds are measured after each cycle of loading and unloading. After each cycle, the damage identification is carried out. Thus the progress of damage is traced by using the estimated results in the last stage as the initial values in the next stage successively.

For the damage identification, two kinds of a priori information are necessary. One is information on the overall degree of inflicted damage, which corresponds to measured natural frequencies which can be extracted from impact sounds using a frequency analysis. In this paper, it is assumed that the measured natural frequencies are approximately equivalent to natural frequencies which represent the dynamic characteristics of the specimen[5),6)]. These frequencies are dependant on the E.M. distribution and calculated by eigen value analysis using a Finite Element Method (FEM) model[7)]. The other is information on the location and relative severity of damage, which is derived from the distribution of estimated AE hypocenters and the failure surface. The estimated AE hypocenters are

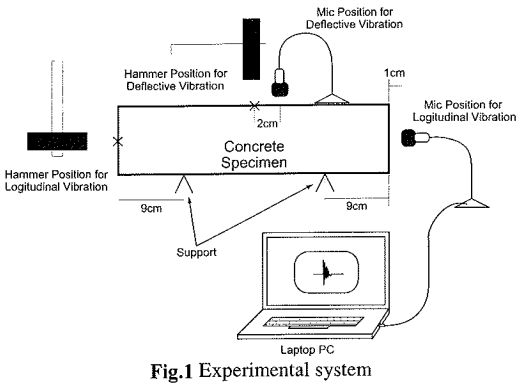

Fig.1 Experimental system

decided upon by using the grid point method[8]. This information on the location and relative severity of damage are transformed into simple indicators which represent the relative degree of damage according to certain criteria, which are explained later and used as a priori information in the damage identification.

Due to the lack of information on real damage, it is not possible to validate the results of the estimated progress of damage. In the paper, several cases are set up to examine the influence of some GA parameters on the inferred progress of damage. By comparing these cases, the validity of this method is confirmed.

2. EXPERIMENT CONDITIONS

(1) Natural Frequency from Impact Sounds

The impact sounds for deflective and longitudinal vibrations are measured using an experimental system shown in **Fig.1**. The support positions of the specimen are immobile points of the 1st deflective natural vibration which are $0.224L$ inward from the edges, where L is the length of the specimen. The impacts are administered manually. Impact sounds are recoded as digital data on a PC with a microphone. The performance of the microphone is shown in **Table 1** and the recording condition is shown in **Table 2**. Because the microphone has a uni-directional character, it is expected that less unwanted sounds are included.

The measured impact sounds are divided into time-series data with a length of 1024 and undertake frequency analysis by the Blackman-Tukey method, which estimates a power spectrum of the time-series data from the Fast Fourier Transform (FFT) of its auto correlation function. Because the frequency resolution in the frequency analysis is 10.8Hz, it is noted that errors of ±5Hz are included in the measured natural frequencies. The measured natural

Table 1 Performance of microphone

Frequency characteristics	10-10000Hz
Sensitivity	-38±3.5dB
SN ratio	56dB

Table 2 Recording condition

Sampling rate	44100Hz
Quantize bit	16 bits

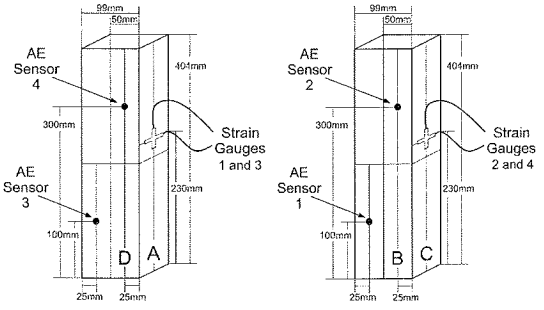

Fig.2 Position of AE sensors and strain gauges (A and C are the facing planes)

Table 3 Mix design of concrete specimen

W/C	Strength	Sand ratio	Air content
0.57	26.7 MPa	41 %	1.5 %

Water	Cement	Sand	Gravel
183 kg	321 kg	752 kg	1064 kg

frequencies are less than 10kHz and are also less than the Nyquist frequency, half of the sampling frequency.

From the past studies[5),6)], it has been confirmed that the measured natural frequencies which can be extracted from impact sounds are approximately the natural frequencies which can be determined from vibration data. Therefore, it can be assumed that they are equivalent.

(2) Acoustic Emissions

The disposition of AE sensors and strain gauges are shown in **Fig.2**. Four AE sensors are used and two sets of vertical and horizontal strain gauges are attached. In measuring AE signals, gain level of the pre-amplifier is set at 40dB and AE signals larger than 45dB are measured. In this paper, the grid point method is implemented to estimate the hypocenters of each AE event which has been measured at three or four sensors. Due to the limitation of the number of available sensors, it is not possible to use the nonlinear least squared method, which is usually used for the estimation of the hypocenters.

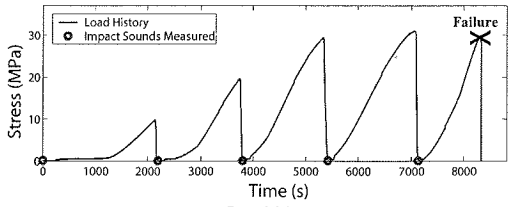

Fig.3 Load history

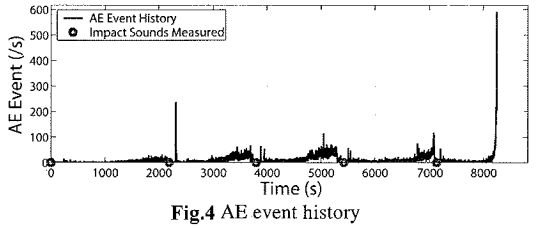

Fig.4 AE event history

Table 4 Measured changes in natural frequencies and the average E.M. of FEM model

Stage	Deflective frequency (Hz)	Longitudinal frequency (Hz)	Average E.M. of FEM model (GPa)
Initial	1841	4372	28.25
1st	1798	4288	27.05
2nd	1766	4200	26.05
3rd	1701	4048	24.20
4th	1637	3866	22.20

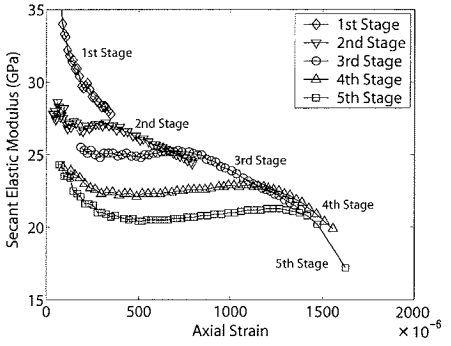

Fig.5 Secant elastic modulus as a function of strain

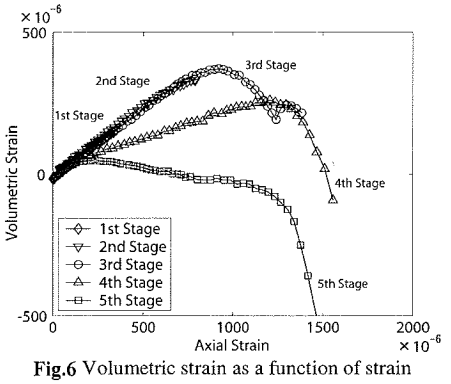

Fig.6 Volumetric strain as a function of strain

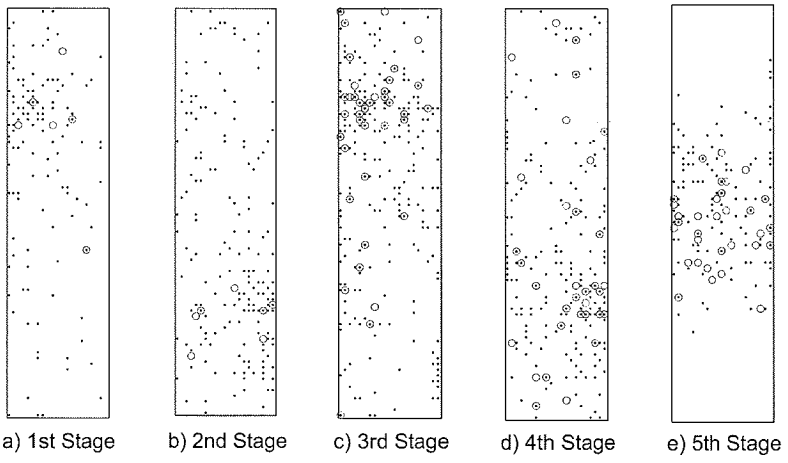

Fig.7 2-D distributions of the estimated AE hypocenters

Photo.1 Failure surface

3. EXPERIMENT RESULTS

(1) AE Event History

The concrete specimen whose mix design is shown in **Table 3** undertakes cyclic uniaxial loading. The load history and the AE event history are shown in **Figs.3** and **4** respectively. There are five loading stages and impact sounds are measured after each stage, which is indicated by a circle in **Fig.3**. In short, measurement of impact sounds is conducted without loading stress in the specimen. This is for measurement of deflective and longitudinal vibrations. It is seen from **Fig.4** that the failure of the specimen has gradually progressed until the 4th loading stage and the specimen failed suddenly at the 5th loading stage.

(2) Mechanical Damage

Secant E.M. and volumetric strain as a function of strain at each loading stage are shown in **Figs.5** and

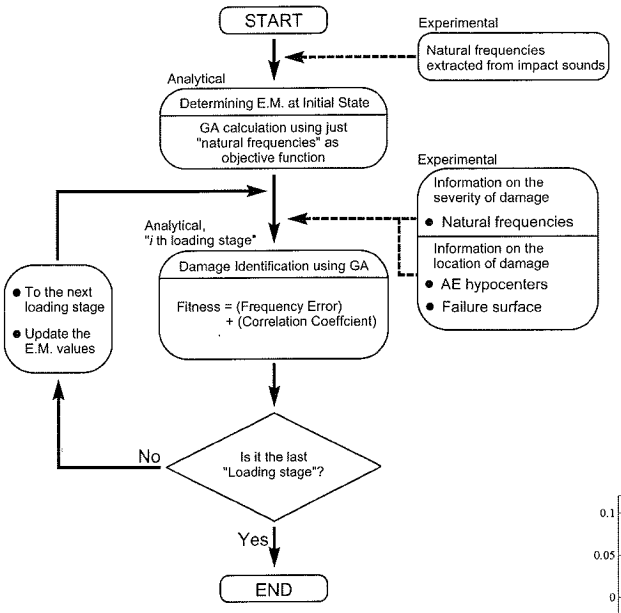

Fig.8 Successive damage identification scheme

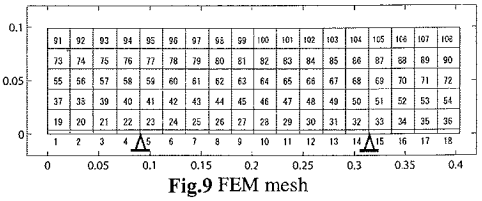

Fig.9 FEM mesh

Table 5 Model parameter

Length (mm)	404
Height (mm)	99
Capping (mm)	4
Poisson's ratio	0.20
Density (kg/m^3)	2250

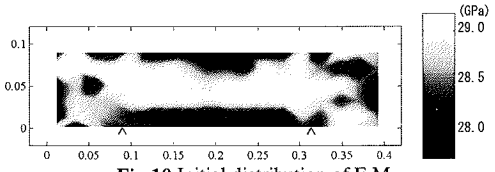

Fig.10 Initial distribution of E.M.

6. The positive volumetric strain means compression. It is found from **Fig.5** that the secant E.M. decreases gradually as the loading stage proceeds, which may indicate the progress of damage. It is seen from **Fig.6**, that the volumetric strain is converted from compression to expansion at the 3rd loading stage. It is expected that the volume increase is caused from the generation of cracks in the specimen. The timing of change in volumetric strain from compression to expansion corresponds to that of the drastic decrease of E.M. in the 3rd loading stage. After that, E.M. decreases up to the same value as the ultimate one in the 4th and 5th loading stage. It is inferred that the drastic progress of damage has begun at this time.

(3) Changes of Measured Natural Frequencies

The deflective and longitudinal natural frequencies analyzed from measured impact sounds at each loading stage and the average E.M. of the FEM model which yields closer values to the measured frequencies, are shown in **Table 4**. The values in the table are averages of frequencies extracted from 10 impact sounds at each loading stage. In the measurement, the coefficient of variation of 10 measured values is less than 0.5%.

It is seen from **Table 4** that both deflective and longitudinal natural frequencies decrease as the loading stage advances. In particular, these greatly decreased at the 3rd and 4th loading stages. It is inferred that the damage has progressed at this time. This result corresponds to the mechanical changes shown in **Figs.5** and **6**. The average E.M. used in the FEM model decreases by 22% after the 4th loading stage from the initial undamaged condition. This also corresponds to the change in measured secant E.M. shown in **Fig.5**.

(4) Estimated AE Hypocenters

By using the grid point method, the AE hypocenters are approximately estimated on the assumption that P-wave velocity is 4050m/s. The 2-D distributions of the estimated AE hypocenters on the B-D surface at each loading stage are shown in **Fig.7**. In addition, **Photo 1** indicates the ultimate situation of the specimen. The AE hypocenters having more than 60dB are plotted. The hypocenters expressed with a dot are obtained from three AE signals and those with a circle are obtained from four AE signals.

It is found from the figure that the damage has progressed from both edges of the failure surface inward and lastly the center parts of the surfaces failed. In comparison with the actual failure surface, it seems that the estimated hypocenters concentrate along the failure surface. In this paper, spatial information on the inflicted damage distribution is obtained from the estimated AE hypocenters by the grid point method.

4. SUCCESSIVE DAMAGE IDENTIFICATION

(1) Methodology

A successive damage identification scheme is shown in **Fig.8**.

Firstly, the initial condition of the specimen is inferred from the measured natural frequencies. The initial distribution of E.M. is obtained from GA by using only the natural frequencies as the objective function. Then the damage identification method, by adding information on the location and severity of damage which is available at each loading stage of the experiment, is carried out. In GA, both a priori information are integrated into an objective function. This method[4] will estimate a decreased degree of E.M. of each element and produce the damage distribution giving the best fitness value (hereafter, the best fitness distribution). In this paper, the measured natural frequencies are used as a priori information on the severity of damage, and the 2-D distribution of the estimated AE hypocenters and failure surface are used as a priori information on the location of damage. The objective function is defined as follows:

$$Fitness = (Frequency\ Error) + (Correlation\ Coefficient) \quad (1)$$

The frequency error in Eq.(1) represents the reciprocal of the sum of the squared error ratio between the calculated natural frequency $f^{(i)}_{calculated}$ and the measured natural frequency $f^{(i)}_{measured}$. The superscript i indicates the i th vibration mode. The frequency error is given by:

$$(Frequency\ Error) = \left\{ \sum_{i=1}^{n} \left(\frac{f^{(i)}_{calculated} - f^{(i)}_{measured}}{f^{(i)}_{measured}} \right)^2 \right\}^{-1} / Cr \quad (2)$$

where, n represents the number of the considered measured natural frequencies. Cr in Eq.(2) is an indicator of squared error ratio. If the squared error ratio of the estimated distribution meets the aimed value, the frequency error will become one.

The correlation coefficient in Eq.(1) represents a factor of the similarity between the estimated distribution of the decrease of E.M. due to the damage and the a priori information of the damage distribution, and is expressed as follows:

$$(Correlation\ Coefficient) = E\left[\frac{C(X_1, X_2)}{\sqrt{C(X_1, X_1) C(X_2, X_2)}} \right] \quad (3)$$

$$C(X_1, X_2) = E[(X_1 - \mu_1)(X_2 - \mu_2)] \quad (4)$$

where $C(X_1, X_2)$ is a covariance matrix. $E[\bullet]$ denotes an expectation operation. X_1 and X_2 are the estimated distribution and the a priori information of E.M. and μ_1 and μ_2 are the average values of X_1 and X_2 respectively. Frequency error and correlation coefficient have a real number from 0 to 1 and hence the fitness value varies from 0 to 2.

After the calculation finishes at a loading stage, the best fitness distribution is selected as the initial damage distribution of the next loading stage. The successive damage identification is examined by repeating these operations up to the last loading stage

(2) Initial Condition

A FEM mesh using a 2-D plane stress element is shown in **Fig.9**. A thin layer at the bottom indicates the capping. Model parameters which are based on the actual specimen are shown in **Table 5**.

Eigen value analysis is implemented to calculate natural frequencies of the two natural vibrations. The 1st deflective and longitudinal vibrations are adopted in the objective function in this paper. This is because the variance of the natural frequencies of the other vibrations is much larger than that of the two adopted vibrations.

Fig.10 shows the initial distribution of E.M., which is identified with the a priori information of only the natural frequency before loading. In the process of GA, the number of coding bits is set at 3 and thus the phenotype has 8 ($=2^3$) levels of E.M.. As the discrete interval of E.M. in genotype, dE, is set at 0.2GPa.

(3) A Priori Information

The 2-D distributions of the AE hypocenters and the assumed failure surface are used as a priori information. The AE hypocenters at each loading stage are transformed with 3 and 4 levels according to the percentage of the hypocenters, which is a ratio of the number of hypocenters in the specific area to that of all hypocenters in each loading stage. The standard for classification is shown in **Table 6.** The resultant 3 and 4 level damage distributions of the estimated AE hypocenters at the 1st loading stage are shown in **Figs.11** and **12**. The assumed failure surface, which is determined from the ultimate situation of the specimen (**Photo 1**) according to the examiner's subjective observation, is also transformed into a priori information with 3 and 4 levels. The elements located at the assumed failure surface have the most severe damage level and the surrounding elements have an intermediate damage level. For instance, in determining the 3-level a priori information of the assumed failure surface,

Table 6 Classification of the AE hypocenter to a priori information

3-level		4-level	
Percentage	Level	Percentage	Level
< 1%	0	< 1%	0
1-4%	1	1-3%	1
> 4%	2	3-5%	2
		> 5%	3

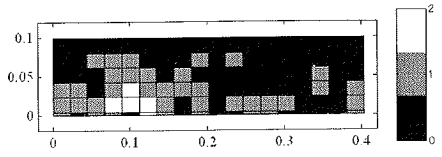

Fig.11 3-level information of the AE hypocenters

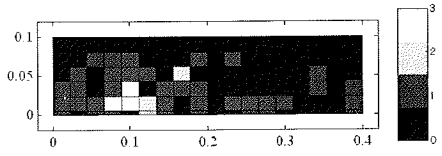

Fig.12 4-level information of the AE hypocenters

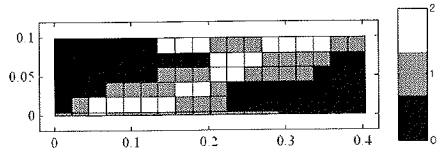

Fig.13 3-level information of the failure surface

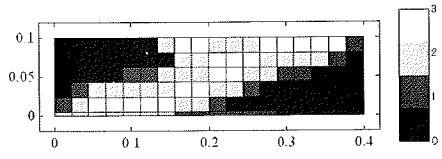

Fig.14 4-level information of the failure surface

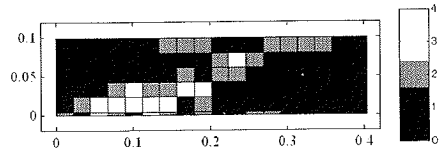

Fig.15 3-level total a priori information (1st stage)

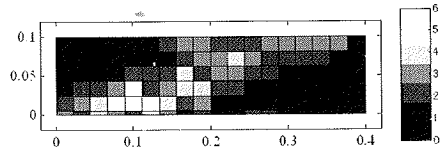

Fig.16 4-level total a priori information (1st stage)

Table 7 Examined cases

Cases	Remarks
Case 1	3-level a priori information for the AE hypocenters and failure surface.
Case 2	4-level a priori information for the AE hypocenters and failure surface.
Case 3	3-level a priori information for the AE hypocenters and failure surface is used. Damage level of the AE hypocenters is weighted as twice as that of the failure surface.
Case *a*	The damaged areas over 0 level are examined.
Case *b*	All elements are examined.
Case α	Either Case *a* or *b* is adopted during all stages.
Case β	At each loading stage, both Cases *a* and *b* are adopted and the result giving a better fitness value is selected.

the elements at the failure surface are represented by 2, those surrounding the failure surface are represented by 1, and those of undamaged areas are represented by 0. These values indicate the relative severity of damage. The 3 and 4 level damage distributions obtained from the failure surface are shown in **Figs.13** and **14**. They are not changed during loading stages.

At each loading stage, total a priori information is defined as the addition of a priori information of the AE hypocenters and that of the failure surface. The 3 and 4 level total damage distributions as a priori information at the 1st loading stage are shown in **Figs.15** and **16**.

(4) Examined Cases

To examine the identification method, three cases of a priori information, two cases of damaged areas,

Table 8 GA parameters at cases and loading stages

Cases		1st stage	2nd stage	3rd stage	4th stage
Case 1-*a*	*dE* (GPa)	0.7	0.7	1.05	1.1
	Candidates	10E36	10E33	10E37	10E38
Case 1-*b*	*dE* (GPa)	0.5	0.4	0.6	0.65
	Candidates	10E60	10E57	10E58	10E60
Case 2-*a*	*dE* (GPa)	0.7	0.7	1.05	1.1
	Candidates	10E44	10E43	10E44	10E46
Case 2-*b*	*dE* (GPa)	0.5	0.5	0.6	0.65
	Candidates	10E66	10E64	10E67	10E69
Case 3-*a*	*dE* (GPa)	0.75	0.7	1.15	1.25
	Candidates	10E42	10E37	10E42	10E44
Case 3-*b*	*dE* (GPa)	0.5	0.5	0.75	0.8
	Candidates	10E62	10E58	10E63	10E64

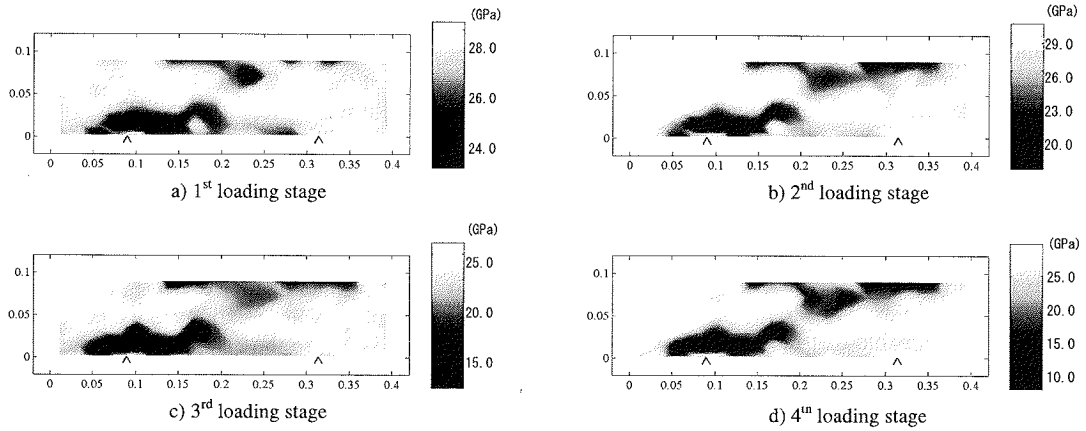

a) 1st loading stage b) 2nd loading stage

c) 3rd loading stage d) 4tn loading stage

Fig.17 Case 1-*a*/*b*-β: Best fitness distributions at loading stages

Table 9 Case 1: Changes in fitness values and E.M. of the best fitness distribution at each loading stage

	1st stage		2nd stage		3rd stage		4th stage	
	Max. fitness	Ave. E.M. (GPa) (Max., Min.)	Max. fitness	Ave. E.M. (GPa) (Max., Min.)	Max. fitness	Ave. E.M. (GPa) (Max., Min.)	Max. fitness	Ave. E.M. (GPa) (Max., Min.)
Case 1-*a*-α	1.948	27.67 (29.05,22.75)	1.976	26.77 (29.05,18.95)	1.935	25.59 (29.05,11.60)	1.887	24.35 (29.05,9.40)
Case 1-*b*-α	1.913	27.6 (29.05,24.15)	1.940	26.83 (29.05,21.75)	1.887	25.51 (28.85,17.55)	1.210	23.98 (28.20, 15.60)
Case 1-*a*/*b*-β	1.948	27.67 (29.05,22.75)	1.976	26.77 (29.05,18.95)	1.935	25.59 (29.05,11.60)	1.890	24.24 (29.05,9.65)

and two cases of searching methods of the best fitness distribution are examined. The examined cases are explained in **Table 7**.

Because the number of coding bits in the genotype for each element is set at 3 and thus 2^3 levels in phenotype are used, *dE* varies according to the differences in Case *a* or *b*. At each loading stage, the best fitness distribution is searched for, by using both Cases *a* and *b* on damaged areas. Then, Cases α and β are used.

To summarize the above-mentioned process, firstly, Cases 1-3 related to a priori information are decided upon to examine the influence of transformation procedures of a priori information. In each case, Case *a* which searches damage distributions in localized areas and Case *b* which searches those in a whole area are then used. The best fitness distribution for the next loading stage is decided according to Case α or β. When Cases *a* and α are adopted in successive identification, the most localized damage distribution is obtained. When Case β is adopted, the damage distribution having the best fitness at each loading stage is obtained. There are three combinations: *a*-α, *b*-α, and *a*/*b*-β. Therefore nine combinations are

examined in total.

The GA parameters (dE and the number of candidates) at the loading stage for each case are shown in **Table 8**. The population and the upper limit of generations are set to 30 and 100 respectively. In addition, the Cr in Eq.(2) is set to 40000 in all the cases, which requires an error ratio of ±0.35%.

(5) Results

a) Case 1

The best fitness distributions at each loading stage of Case 1-a/b-β are shown in **Fig.17**. In Case 1, the 3-level a priori information is used for both the AE hypocenters and failure surface. The fitness value of the best fitness distribution and the average, maximum and minimum E.M. of the best fitness distribution at each loading stage are shown in **Table 9**. Tracking the change of the average E.M. of the best fitness distribution is useful to understand the changes of secant E.M. and natural frequencies in the experiment. Also, the change of maximum and minimum E.M. is a useful indicator to trace the localized progress of damage.

It is found from **Fig.17** that the damage is greatly localized and the E.M. at the damage zone decreases gradually. It is notable that the value of the contour bar becomes smaller, which means a decrease of the minimum E.M. and also a decrease of the average E.M.. In Case β, Case a was selected at the 1st-3rd loading stages and Case b was selected at the 4th loading stage. In general, it is found that Case a produces a better fitness value than Case b. The minimum E.M. at the 4th loading stage resulted in 9.4GPa.

b) Case 2

The best fitness distributions at each loading stage of Case 2-a/b-β are shown in **Fig.18**. In Case 2, the 4-level a priori information is used for both the AE hypocenters and failure surface. The fitness value of the best fitness distribution and the average, maximum and minimum E.M. of the best fitness distribution at each loading stage are shown in **Table 10**.

Comparing with **Fig.17**, it is found that the difference between maximum and minimum E.M. in Case 2-a/b-β is smaller than that in Case 1-a/b-β, while the average E.M. is a little larger. The best fitness value in Case 2-a/b-β is smaller than that in Case 1-a/b-β in general. In Case β, Case a was selected at the 1st and 2nd loading stages and Case b was selected at the 3rd and 4th loading stages. The minimum E.M. at the 4th loading stage resulted in 11.0GPa.

c) Case 3

The best fitness distributions at each loading stage of Case 3-a/b-β are shown in **Fig. 19**. In Case 3, the 3-level a priori information is used for both the AE hypocenters and failure surface and the damage level of the AE hypocenters is weighted as twice that of the failure surface, which means that a priori information on the location of damage is poor. The fitness value of the best fitness distribution and the average, maximum and minimum E.M. of the best fitness distribution at each loading stage are shown in **Table 11**.

Comparing with **Figs.17** and **18**, it is found that the progress of damage in Case 3-a/b-β happens in smaller areas than that in the other cases. This is probably because of the influence of the large weight of the AE hypocenters. In Case β, Case a was selected at the 1st-3rd loading stages and Case b was selected at the 4th loading stage. The minimum E.M. at the 4th loading stage resulted in 9.65GPa.

5. CONCLUSIONS AND DISCUSSIONS

This paper applied the damage identification method using GA, whose validity is examined in the companion paper[4], to the estimation problem of the progress of damage in a rectangular concrete specimen due to cyclic uniaxial loading. From the experiment, the natural frequencies, the AE hypocenters and the failure surface are obtained. These data are transformed into simple indicators of the relative degree of damage and used as a priori information in the successive damage identification method. From the results of this examination, the following observations and conclusions can be made:

1. The change in the measured natural frequencies corresponds well to that in mechanical properties. In addition, the distribution of the AE hypocenters from the grid point method corresponds well to the actual failure surface. It is expected that the combination of impact acoustics method and AE method is effective to estimate the progressive failure.
2. When the resolution degree of a priori information is high, the fitness value decreases. This is probably because the number of candidates becomes large, and it becomes difficult to converge the fitness value. If the population and the upper limit of generations are set at a high value, the fitness value will be high in the case of the high resolution degree of a priori information. This is, however, not effective in an actual case.

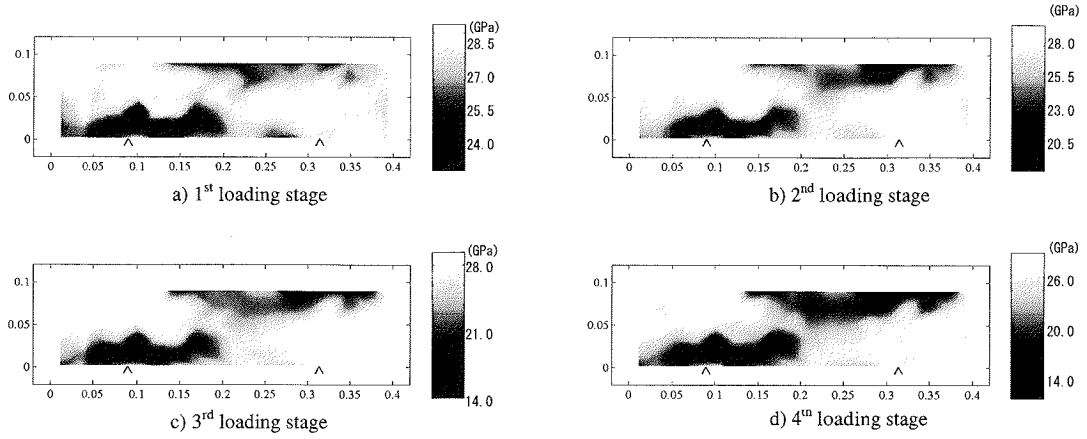

a) 1st loading stage b) 2nd loading stage

c) 3rd loading stage d) 4tn loading stage

Fig.18 Case 2-*a*/*b*-*β*: Best fitness distributions at each loading stage

Table 10 Case 2: Changes in fitness values and E.M. of the best fitness distribution at each loading stage

	1st stage		2nd stage		3rd stage		4th stage	
	Max. fitness	Ave. E.M. (GPa) (Max., Min.)	Max. fitness	Ave. E.M. (GPa) (Max., Min.)	Max. fitness	Ave. E.M. (GPa) (Max., Min.)	Max. fitness	Ave. E.M. (GPa) (Max., Min.)
Case 2-*a*-*α*	1.891	27.57 (29.05,23.15)	1.923	26.72 (29.05,18.95)	1.908	25.50 (29.05,12.65)	1.876	24.16 (29.05,11.0)
Case 2-*b*-*α*	1.829	27.49 (29.05,24.15)	1.902	26.57 (29.05,21.45)	1.914	25.20 (28.85,17.85)	1.885	23.98 (29.05, 13.95)
Case 2-*a*/*b*-*β*	1.891	27.57 (29.05,23.15)	1.923	26.72 (29.05,18.95)	1.915	25.37 (29.05,14.75)	1.885	24.24 (29.05,12.15)

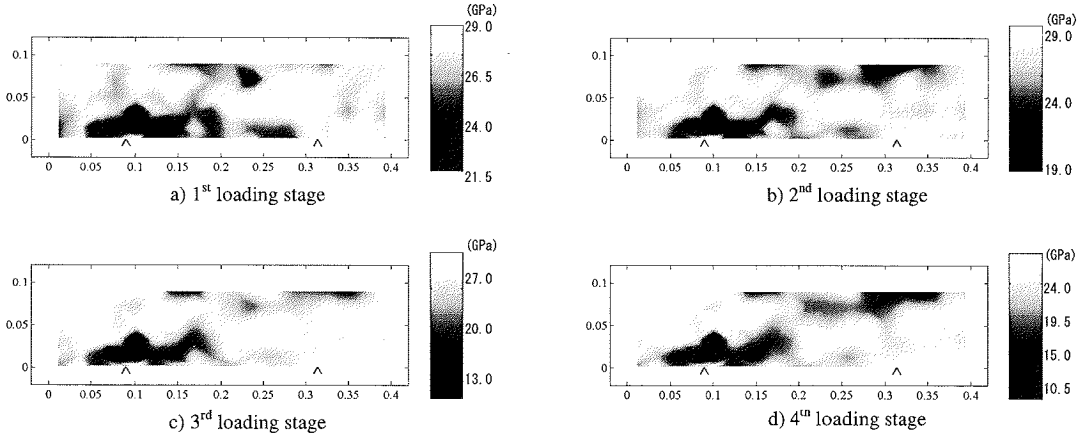

a) 1st loading stage b) 2nd loading stage

c) 3rd loading stage d) 4tn loading stage

Fig.19 Case 3-*a*/*b*-*β*: Best fitness distributions at each loading stage

Table 11 Case 3: Changes in fitness values and E.M. of the best fitness distribution at each loading stage

	1st stage		2nd stage		3rd stage		4th stage	
	Max. fitness	Ave. E.M. (GPa) (Max., Min.)	Max. fitness	Ave. E.M. (GPa) (Max., Min.)	Max. fitness	Ave. E.M. (GPa) (Max., Min.)	Max. fitness	Ave. E.M. (GPa) (Max., Min.)
Case 3-*a*-*α*	1.933	27.53 (29.05,22.40)	1.975	26.69 (29.05,19.30)	1.927	25.43 (29.05,11.25)	1.866	23.92 (29.05,10.0)
Case 3-*b*-*α*	1.897	27.51 (29.05,24.15)	1.948	26.61 (29.05,21.45)	1.897	25.12 (29.05,16.20)	1.875	23.56 (29.05,13.8)
Case 3-*a*/*b*-*β*	1.933	27.53 (29.05,22.40)	1.975	26.69 (29.05,19.30)	1.927	25.43 (29.05,11.25)	1.872	23.77 (29.05,9.65)

3. When there is a shortage of a priori information on the location of damage the estimated damaged areas become small. However, the entire profile of the damage zone is similar to that of the case having enough information on the location. It is expected from this result that the proposed method will be effective even if the location of the failure is very difficult to infer.
4. In Case β where the best fitness distribution to the next loading stage is selected among both Cases a and b, Case a is mostly selected at the early loading stages and Case b is mostly selected at the latter. From this, it can be inferred that the progress of damage changes from localized to entire as the failure approaches.

Through the application of this method to the experimental problem, the efficiency of this method is verified. The advantage of this method is that it is robust against errors and noises, compared to other damage identification methods. In addition, this method can integrate several different types of information into one. In actual situations, this method can be used to integrate results from long term structural monitoring with those from periodic and detailed inspections. As is verified in the companion paper[4], better a priori information produces better estimation accuracy. Therefore, it is essential for enhancement of applicability and efficiency of this method to improve accuracy of individual monitoring and inspection technique.

For the future, it is important to define an objective function which has specific and physical meaning and to establish more objective standards for transforming experimental data into simple indicators of the relative degree of real damage. It is also expected that this method will be applied to other experimental problems and actual situations to refine its effectiveness.

REFERENCES

1) Doebling, H. L., Farrar, C. R., Prime, M. B., and Shevits, D. W.: Damage identification and health monitoring of structural and mechanical systems from changes in their vibration characteristics: A literature review, *Research Rep.*, No. LA-13070-MS, ESA-EA, Los Alamos National Laboratory, 1996.
2) Ren, W. X. and De Roeck, G.: Structural damage identification using modal data. I: Simulation verification, *J. Struct. Eng.*, ASCE, Vol. 128, No. 1, pp.87-95, 2002.
3) Goldberg, D. E.: Genetic algorithms in search, optimization, and machine learning, *Addison-Wesley*, 1989.
4) Goda, K., Kobayashi, A. and Aoyama, S.: Fundamental effectiveness of structural damage identification using genetic algorithm, *J. Materials, Conc. Struct. Pavement*, JSCE, 2003 (submitted).
5) Ito, Y. and Uomoto, T.: Impact acoustics of reinforced concrete beams with cracks, *J. Materials, Conc. Struct. Pavement*, JSCE, Vol. 35, No. 564, pp.169-176, 1997 (in Japanese).
6) Kamada, T., Asano, M., Kunieda, M. and Rokugo, K.: Quantitative nondestructive evaluation of defects in concrete surface layer by impact acoustics methods, *J. Materials, Conc. Struct. Pavement*, JSCE, Vol. 55, No.704, pp.65-79, 2001 (in Japanese).
7) Kwon, Y.W. and Bang, H.: The finite element method using MATLAB, 2nd ed., *CRC Press*, 2000.
8) Ishida, T.: Science of acoustic emission in bedrock, *Kinmirai Press*, 1999 (in Japanese).

(Received March 6, 2003)